

Molecular Physics

An International Journal at the Interface Between Chemistry and Physics

ISSN: 0026-8976 (Print) 1362-3028 (Online) Journal homepage: <https://www.tandfonline.com/loi/tmph20>

Impact of intermolecular vibrational coupling effects on the sum-frequency generation spectra of the water/air interface

Naveen Kumar Kaliannan, Andres Henao Aristizabal, Hendrik Wiebeler, Frederik Zysk, Tatsuhiko Ohto, Yuki Nagata & Thomas D. Kühne

To cite this article: Naveen Kumar Kaliannan, Andres Henao Aristizabal, Hendrik Wiebeler, Frederik Zysk, Tatsuhiko Ohto, Yuki Nagata & Thomas D. Kühne (2020) Impact of intermolecular vibrational coupling effects on the sum-frequency generation spectra of the water/air interface, *Molecular Physics*, 118:4, 1620358, DOI: [10.1080/00268976.2019.1620358](https://doi.org/10.1080/00268976.2019.1620358)

To link to this article: <https://doi.org/10.1080/00268976.2019.1620358>



© 2019 The Author(s). Published by Informa UK Limited, trading as Taylor & Francis Group



[View supplementary material](#)



Published online: 22 May 2019.



[Submit your article to this journal](#)



Article views: 1344



[View related articles](#)



[View Crossmark data](#)



Citing articles: 3 [View citing articles](#)

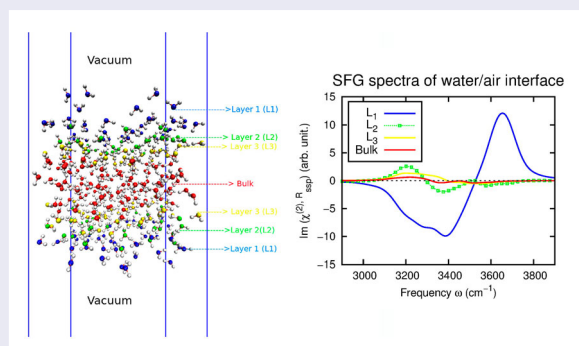
Impact of intermolecular vibrational coupling effects on the sum-frequency generation spectra of the water/air interface

Naveen Kumar Kaliannan^a, Andres Henao Aristizabal^a, Hendrik Wiebeler^a, Frederik Zysk^a, Tatsuhiko Ohto^b, Yuki Nagata^c and Thomas D. Kühne^{a,d}

^aDynamics of Condensed Matter and Center for Sustainable Systems Design, Chair of Theoretical Chemistry, University of Paderborn, Paderborn, Germany; ^bGraduate School of Engineering Science, Osaka University, Toyonaka, Osaka, Japan; ^cMax-Planck Institute for Polymer Research, Mainz, Germany; ^dPaderborn Center for Parallel Computing and Institute for Lightweight Design, University of Paderborn, Paderborn, Germany

ABSTRACT

We have examined the impact of intermolecular vibrational coupling effects of the O-H stretch modes, as obtained by the surface-specific velocity-velocity correlation function approach, on the simulated sum-frequency generation spectra of the water/air interface. Our study shows that the inclusion of intermolecular coupling effects within the first three water layers, i.e. from the water/air interface up to a distance of 6 Å towards the bulk, is essential to reproduce the experimental SFG spectra. In particular, we find that these intermolecular vibrational contributions to the SFG spectra of the water/air interface are dominated by the coupling between the SFG active interfacial and SFG inactive bulk water molecules. Moreover, we find that most of the intermolecular vibrational contributions to the spectra originate from the coupling between double-donor water molecules only, whereas the remaining contributions originate mainly from the coupling between single-donor and double-donor water molecules.



ARTICLE HISTORY

Received 18 March 2019
Accepted 10 May 2019

KEYWORDS



Partially adiabatic centroid
molecular dynamics;
sum-frequency generation;
water/air interface


1. Introduction

The characterisation of liquid water at aqueous interfaces is complex but essential for understanding physicochemical, environmental and biological processes such as organic catalysis on water [1], protein folding [2], atmospheric chemistry [3], electrochemical processes in aqueous batteries [4] and the function of biological membranes, as well as membrane proteins [5]. Among the various aqueous interfaces, the water/air interface is of special interest since it represents a well-studied

model system for aqueous interfaces in general [6–8], which is why it is a good starting point for the present investigation.

Surface-sensitive vibrational sum-frequency generation (SFG) is presently one of the widely employed technique to characterise molecules directly at liquid interfaces [9–12]. The surface-sensitivity is due to the fact that it does not provide a signal in centrosymmetric or isotropic bulk media and is only active at interfaces or surfaces, where the symmetry is broken.

CONTACT Thomas D. Kühne  tdkuehne@mail.upb.de  Dynamics of Condensed Matter and Center for Sustainable Systems Design, Chair of Theoretical Chemistry, University of Paderborn, Warburger Str. 100, D-33098 Paderborn, Germany; Paderborn Center for Parallel Computing and Institute for Lightweight Design, University of Paderborn, Warburger Str. 100, D-33098 Paderborn, Germany

 Supplemental data for this article can be accessed here. <https://doi.org/10.1080/00268976.2019.1620358>

© 2019 The Author(s). Published by Informa UK Limited, trading as Taylor & Francis Group

This is an Open Access article distributed under the terms of the Creative Commons Attribution-NonCommercial-NoDerivatives License (<http://creativecommons.org/licenses/by-nc-nd/4.0/>), which permits non-commercial re-use, distribution, and reproduction in any medium, provided the original work is properly cited, and is not altered, transformed, or built upon in any way.

In recent years, this technique has been very successful in providing vibrational spectra for various interfacial systems [13–18]. Among those, the water/air interface has been the most intensively studied system, both experimentally [18–26] and theoretically [11,18,25–36]. However, the interpretation of the experimental SFG spectra of the water/air interface in the spectroscopic range between 3000 and 3600 cm^{-1} is still a matter of great debate [11,19,22,25,30,34,36–38]. In this regard, theoretical SFG simulations have been employed to assist the interpretation and assignment of the O-H stretch vibrational features in the experimental SFG spectra [11,14,18,27,30,36,38,39]. Typically, these simulations include intra- and intermolecular vibrational couplings of O-H stretch modes [40–43], which strongly affects the speed and time scales of spectral diffusion and alters the SFG response of the O-H stretch frequency [18,22]. Yet, in practical SFG simulations, only the intramolecular vibrational coupling effects are explicitly included, while the intermolecular vibrational couplings are generally neglected [11,28,44,45], or just partially treated using a short correlation cutoff [27]. An alternative approach to compute SFG spectra is via the dipole moment-polarisability (μ - α) time-correlation function (TCF) [25,28,30], which however is computationally rather expensive since it requires relatively long trajectories (several ns) to reach numerical convergence [11]. This convergence issue has limited the usage of computationally expensive quantum-mechanical *ab-initio* and path-integral molecular dynamics (MD) simulations to obtain and interpret SFG spectra [46–49]. Nevertheless, recently a few studies have incorporated sufficiently long MD trajectories to study both of these coupling effects [11,18,27,30,31]. In particular it has been shown that intramolecular coupling effects gives rise to the vibrational O-H stretch response in the SFG spectra, while the intermolecular couplings induces a red-shift in the H-bonded O-H stretch response. Moreover, it has been shown that the intermolecular coupling induced SFG features in the spectra are in good agreement with experimental SFG spectra [18,27,30].

In the present study, the surface-specific velocity-velocity correlation function (ssVVCF) method, which was recently developed by some of us [11], has been employed. The chief advantage of this approach is the up to an order of magnitude faster convergence than the usual μ - α TCF scheme. Using this approach allows us to obtain well converged SFG spectra of the water/air interface in order to assess the impact of intermolecular coupling effects. For the purpose to demonstrate the significance of intermolecular couplings in the SFG simulations, the obtained SFG spectra are compared with

experimental measurements. Furthermore, we have also employed an instantaneous layer analysis to separate the vibrational contributions arising from interfacial water molecules and to obtain unambiguous contributions to the overall SFG spectra. This instantaneous layer analysis has also allowed us to study intermolecular coupling effects that occur between the O-H stretch modes of the same water layer, as well as in different water layers of the system.

The remaining of this paper is organised as follows. The computational details including the interface definition and the ssVVCF formalism are described in Section 2. Section 3 contains our results and discussion, which is followed by a summary in Section 4.

2. Computational details

2.1. Partially adiabatic centroid molecular dynamics simulations

A total of 250 statistically independent partially adiabatic centroid MD (PA-CMD) simulations of the water/air interface were performed at ambient conditions. In the PA-CMD scheme, the effective masses of the individual replicas that makes up the closed p -bead ring-polymers, which are isomorphic to the original quantum particles [50,51], are adjusted so as to shift the spurious oscillations beyond the spectral range of interest [52]. Specifically, the elements of the Parrinello-Rahman mass matrix are chosen so that the internal modes of the ring-polymer are shifted to a frequency of

$$\Omega = p^{p/p-1} \frac{k_B T}{\hbar}, \quad (1)$$

which allows for the use of integration timesteps similar to that in conventional MD simulations [53].

Throughout the flexible q-TIP4P/F water model of Habershon et al. [52], augmented by the explicit three-body (E3B) interactions proposed by Skinner and coworkers [54], had been employed. We note that the present flexible, but fixed point-charge water model is neither polarisable nor able to mimic cooperativity effects and chemical reactions that may take place in liquid water. Moreover, to be precise, we would like to emphasise that the E3B scheme was originally parametrised for the rigid TIP4P/2005 force-field of Abascal and Vega [55], which forms the basis and is hence very closely related to the used flexible q-TIP4P/F water model [52]. The simulated water slab consisted of 343 water molecules in an orthorhombic simulation cell of lengths 21.75 Å \times 21.75 Å \times 108.75 Å, respectively. To mimic the water/vapor interface, the supercell approach

was employed by adding a 43.5 Å long vacuum portion on both sides of the system along the non-periodic z -direction and applying periodic boundary conditions. Short-range interactions were truncated at 9 Å, whereas the Ewald summation technique was employed to treat the long-range electrostatic interactions. To explicitly consider nuclear quantum effects (NQE) in a computationally efficient way, the ring polymer contraction scheme was used with a cutoff value of $\sigma = 5$ Å to reduce the electrostatic potential energy and force evaluations to a single Ewald sum, in order to speed up the calculations [52]. This is to say that 32 ring-polymer beads were employed to converge all relevant properties [47,52,56–60], while the computationally expensive part of the electrostatic interactions were contracted to the centroid only. In all simulations, using a discretised integration timestep of 0.1 fs, the system was first equilibrated 10 ps in the canonical ensemble, before microcanonical ensemble averages were computed over the following 8 ps, resulting in a total statistics of 2 ns to compute the present SFG spectra.

2.2. Interface definition

In order to decompose the eventual SFG spectra into its contributions of the different interfacial water layers, we first determine all water molecules that belong to the interfacial region of the water/vapour interface within all our trajectories and their corresponding residence times. Several techniques [61–64] and definitions [65–67] have been developed in the past to define the interfacial region and to identify the interfacial molecules. Here, the so-called Identification of the Truly Interfacial Molecules scheme is employed to unambiguously identify the water molecules that are truly located at the boundary of the two different phases at every timestep [61,63,64]. This technique determines the instantaneous interfacial water molecules by moving a probe sphere of a given radius R_{ps} along a set of lines that are perpendicular to the plane of the interface. All molecules hit by the probe spheres are considered as interfacial water molecules, whereas the position of the spheres when they are in contact with the interfacial molecules is defined to be the location of the instantaneous interface. Moreover, this technique also permits to unambiguously identify the molecules forming the successive (second, third, etc.) water layers by repeating the same procedure without the already identified molecular layer [61,63,64]. Throughout the present work, a probe sphere radius of $R_{ps} = 2$ Å has been used to identify the molecules in the topmost (L_1), second (L_2) and third (L_3) layer of water, whereas all remaining molecules are considered to be the bulk water.

2.3. SFG spectra calculations

The resonant term of the second order non-linear susceptibility is calculated using the ssVVCf formalism, pioneered by some of us [11]. The equation used to calculate the resonant term in this work is given by

$$\chi_{abc}^{(2),R}(\omega) = \begin{cases} \frac{Q(\omega)}{i\omega^2} \int_0^\infty dt e^{-i\omega t} \\ \times \left\langle \sum_{ij} g_t(r_{ij}(0); r_t) \right. \\ \left. \dot{r}_{c,i}^{\text{OH}}(0) \frac{\dot{r}_j^{\text{OH}}(t) \cdot \ddot{r}_j^{\text{OH}}(t)}{|\ddot{r}_j^{\text{OH}}(t)|} \right\rangle, & \text{if } a = b \\ 0, & \text{otherwise,} \end{cases} \quad (2)$$

where $r_{ij}(t)$ is the distance between the centre of masses of O-H groups i and j at time t , whereas $g_t(r_{ij}; r_t)$ is the function to control the cross-correlation terms with the cross-correlation cutoff radius of r_t . The intramolecular distances and velocities of O-H group j at time t are denoted as $r_j^{\text{OH}}(t)$ and $\dot{r}_j^{\text{OH}}(t)$, respectively. The quantum correction factor $Q(\omega)$ was taken from Ref. [11] and the Hann window function was applied for the Fourier transformation of the TCF. Even though non-Condon effects are neglected, all intramolecular coupling effects are included in terms of the auto-correlation (Auto-C) and intramolecular cross-correlation (Intra-CC) function, whereas the intermolecular coupling is included using the intermolecular cross-correlation (Inter-CC) function of the O-H stretch modes. Nevertheless, it is important to realise that within this formalism, the amount of correlation is increasing by enlarging r_t . For example, when $r_t = 0$ Å, only the auto-correlation of O-H stretch modes is included. However, increasing r_t to 2 Å entails the correlations within a water molecule, that is the auto-correlation and the intramolecular cross-correlation, but no intermolecular cross-correlation. However, only for r_t much greater than 2 Å, all three three correlation contributions are explicitly taken into account. Although in the latter case, the present ssVVCf technique is generally more accurate and computationally much cheaper than the conventional μ - α TCF approach [11], it still requires rather long trajectories to obtain unbiased SFG spectra.

Hence, in this work, we first assessed the necessary trajectory length to get unbiased SFG spectra with minimal variance as quantified by the standard error of the mean (SEM). The spectra, which are shown in Figure 1, are computed for three different cutoff radii ($r_t = 0$ Å, 2 Å and 6 Å) to demonstrate the impact of r_t on the eventual result and on the required minimal trajectory length. We found that for $r_t = 0$ Å and 2 Å respectively, a

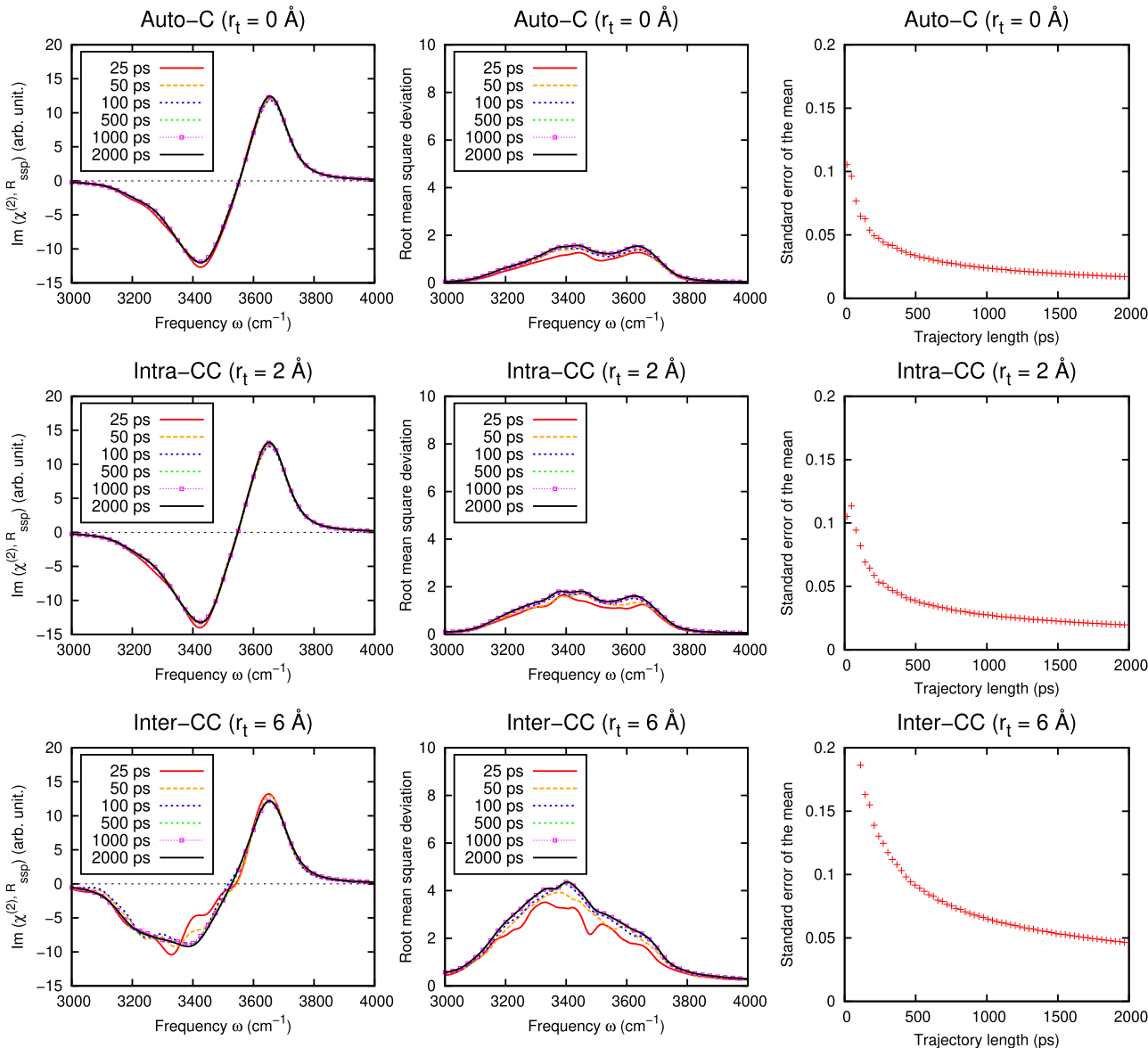


Figure 1. Simulated O-H stretch SFG spectra as a function of trajectory lengths (left panel), root mean square deviation within the SFG spectral region between 3000–4000 cm^{-1} (middle panel) and standard error of the mean (right panel). In the first row just the Auto-C contribution is shown, whereas in the second row the Intra-CC correlation term is added and in the third row also the Inter-CC contribution, respectively.

trajectory length of 100 ps is good enough to converge the statistical uncertainties of the corresponding SFG spectra. Therefore, relatively short trajectories are sufficient for a converged SFG calculation with auto-correlation and intramolecular cross-correlation terms. But, in the case of $r_t = 6 \text{ \AA}$, the SEM is very slowly decaying leading to the oscillations that are visible in the spectral range 3000–3600 cm^{-1} . This is to say that for large values of r_t , the convergence with respect to the trajectory is slower, which is why at least 500 ps are required. In other words, the convergence within the present ssVVCF methods, is highly dependent on the intermolecular cross-correlation term. However, in contrast to a previous work [11], which has not been able to observe any advantage

in terms of accuracy using larger values of r_t , we find that even though the convergence of the ssVVCF method is somewhat slower, the results can be nevertheless systematically improved by increasing r_t at moderate trajectory lengths, given that the window length to compute the TCF is chosen to be small. Based on these results, all following SFG calculations were based on a trajectory length of 200 ps, except for the calculations with $r_t \gg 2 \text{ \AA}$, where 1000 ps was used in order to achieve well converged SFG spectra. Throughout a window length of ~ 1 ps was employed during which the set water molecules were kept fixed. As can be seen in Figures S1 and S2 of the supporting information, this does not lead to any bias in the eventual SFG spectra.

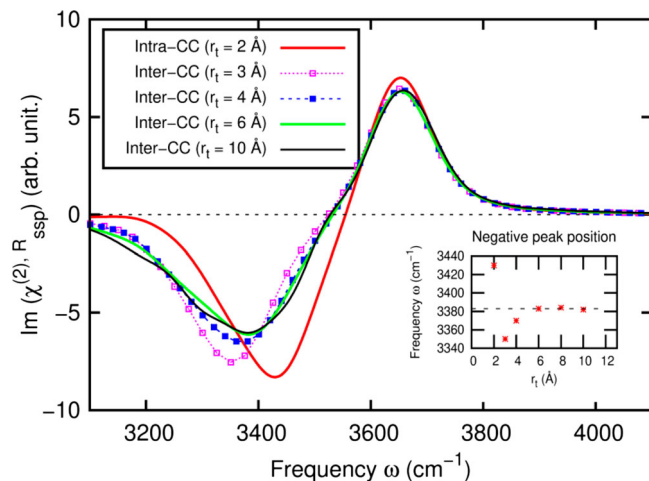


Figure 2. Simulated O-H stretch SFG spectra of the water/air interface, as a function of correlation cutoffs r_t . The inset shows the peak position of the negative peak as a function of r_t .

In addition, we have also studied the impact of the intermolecular coupling effect on the SFG spectra of water/air interface by varying r_t from 3 to 10 Å, as shown in Figure 2. By visual inspection it can be seen that there are substantial differences when increasing r_t up to 3 Å, and smaller ones between 4 to 10 Å. However, a closer inspection of the negative peak position, which is shown in the inset of Figure 2, shows that the latter is not quite converged until r_t is at least 6 Å. This is to say that a much larger value of r_t than previously suggested is necessary to explicitly include all relevant intermolecular vibrational coupling effects within the SFG spectra. Hence, in this work, we set $r_t = 6$ Å, which is also in agreement with the distance of water molecules in the third layer and the instantaneous water surface.

3. Results and discussion

The time-averaged density profiles of the identified water layers (L_1 – L_3) and the full water/air interface system as a function of z -coordinate are shown in Figure 3. Beyond L_3 , the particle density $\rho(z)$ resumes its original bulk value, which is why we simply denoted it as bulk water. The interface is usually defined as the region where the density varies from 95% to 5% of the bulk density, whereas the position so called Gibbs dividing surface is defined as the location where the average density equals 50% of the bulk density [46]. According to this definition, the thickness of the interface and the location of the Gibbs dividing surface are ~ 3.7 Å and 10.65 Å, respectively. However, contrary to the former, the latter definition uses just the averaged interface instead of the instantaneous interface. As a consequence, it does not take water molecules that dynamically switches between L_1 , L_2 , and

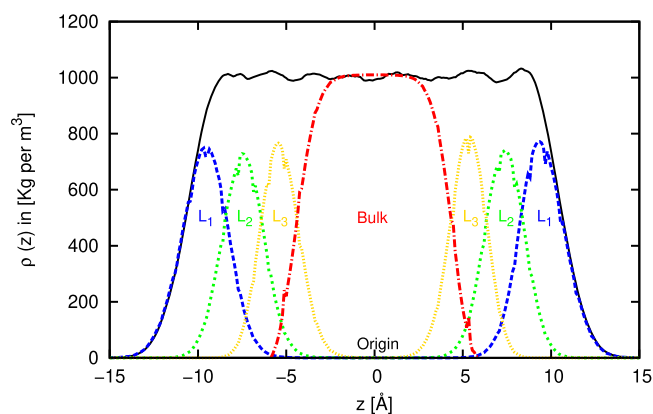


Figure 3. Density profiles of the identified instantaneous water layers (L_1 – L_3) as a function of the z -coordinate, as well as of the full water/air interface.

L_3 at different times explicitly into account, as opposed to the instantaneous interfacial profiles of Figure 3. Therein, the density profiles of the individual layers follow the Gaussian distribution, whose average location and width can be easily characterised by using their peak position and full width at half-maximum that are (± 9.6 Å, 2 Å), (± 7.5 Å, 2 Å) and (± 5.4 Å, 2 Å) for the (center position, width) of layers L_1 , L_2 , and L_3 , respectively. Hence, the identified first water layer extends from the instantaneous interface to a distance of 2.0 Å towards the bulk, whereas the second water layer ranges from 2.0 Å to 4.0 Å and the third water layer from 4.0 to 6.0 Å from the instantaneous interface, respectively.

For the purpose to determine the interfacial thickness of the water/air interface based on the SFG selection rule, we computed the SFG spectra individual as a function of water layer, as shown in Figure 4. The SFG signal is detected from the water molecules in the top most layer (i.e. the sum of L_1 and L_2) only that extend from the instantaneous interface to a distance of 4 Å towards the bulk. Beyond 4 Å, the intensity of the signal becomes almost zero as a result of the centrosymmetrical orientation of the corresponding water molecules that is why we consider the interfacial thickness of the water/air interface to be 4 Å, which is very close to the value of the previous MD simulations [46,47,68,69]. Therefore, only the water molecules in the first two layers are considered as the interfacial molecules from this point on.

The simulated O-H stretch SFG spectra of the interfacial molecules at the water/air interface are shown in Figure 5. In these spectra, we observe a sharp positive peak centred at ~ 3650 cm^{-1} that corresponds to the O-H stretch vibration of the dangling O-H groups pointing out of the water into the vacuum and a broad negative peak in the ~ 3000 – 3550 cm^{-1} range, which corresponds to the O-H stretch vibration of H-bonded O-H

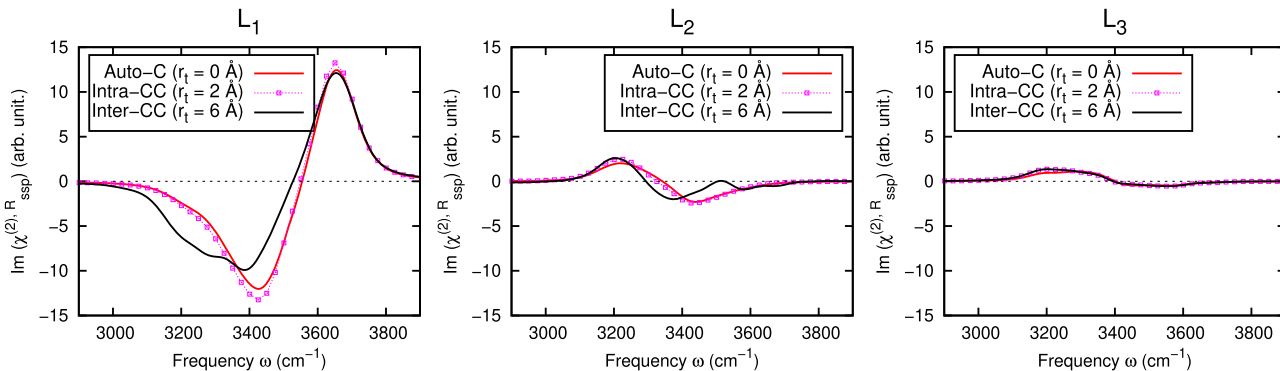


Figure 4. Simulated O-H stretch SFG spectra as a function of r_t for L_1 (left panel), L_2 (middle panel) and L_3 (right panel).

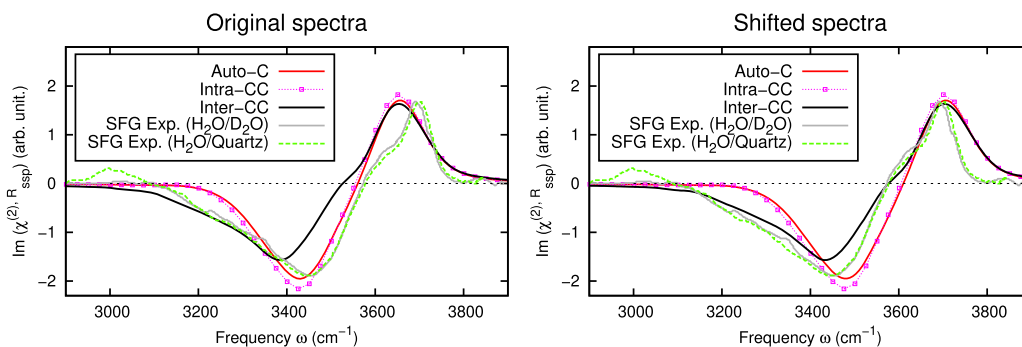


Figure 5. Simulated O-H stretch SFG spectra of the water/air interface in terms of the three different correlation terms. The experimental data refers to the usage of D_2O and crystalline quartz as a reference to calibrate the phase and amplitude, respectively [21]. The original SFG spectra are shown in the left panel, whereas in the right panel the peak of the dangling O-H SFG signal was shifted to the corresponding experimental peak position, i.e. by 50 cm^{-1} .

groups pointing towards the bulk. After blue-shifting the simulated spectra by 50 cm^{-1} , the peak positions as well as the intensities are both in nearly quantitative agreement with the experimental data [21]. The only exception is the high frequency region of the dangling O-H peak, where our simulations does not fully reproduce the experimental measurements. Moreover, the shape of the shoulder in the dangling O-H peak is not quantitatively reproduced. In fact, it has been previously reported that the shape of the shoulder cannot be exactly reproduced by the ssVVCF method [11], but only using the direct μ - α TCF approach. Yet, the positive signal at $\sim 3000\text{ cm}^{-1}$, found in SFG experiments using crystalline quartz as a reference [21], is not present in our SFG spectra. Nevertheless, this signal was found to be a bias originating from the contamination and/or adsorbed water on the quartz surface that inevitably affects the quartz reference signal [21,23]. It was also reported that quartz as a reference surface within SFG measurements of the liquid water can generate an additional phase error, which again induces this $\sim 3000\text{ cm}^{-1}$ positive signal [21]. In any case, including the Inter-CC effects, the present SFG spectra are in nearly quantitative agreement with those

obtained using the more sophisticated many-body potential by Paesani and coworkers [30], as well as *ab-initio* MD simulations of Sulpizi and Gaigeot [27,28,68].

First, we analyse the changes in both peaks in terms of the correlation terms: The dangling O-H peak remains almost unaffected, while the H-bonded O-H peak changes when the intermolecular cross-correlation term is added. As is apparent from Figure 5, introducing the intermolecular cross-correlation term results in a shift of the H-bonded O-H peak position by 50 cm^{-1} from 3430 cm^{-1} to 3380 cm^{-1} . Moreover, the intermolecular cross-correlation term entails a slightly decreased SFG signal in the range of $3380\text{--}3600\text{ cm}^{-1}$ and at the same time enhanced amplitude between $3000\text{--}3380\text{ cm}^{-1}$. This is to say that the inclusion of the intermolecular vibrational coupling effects as obtained by the intermolecular cross-correlation term is essential for the ssVVCF method to reproduce the experimental SFG spectra of the water/air interface. Second, in comparison to previous theoretical studies that have observed a sizable enhancement of the negative peak at $\sim 3000\text{--}3350\text{ cm}^{-1}$ induced by intermolecular coupling effects [11,18,27], our results entails only a smaller such

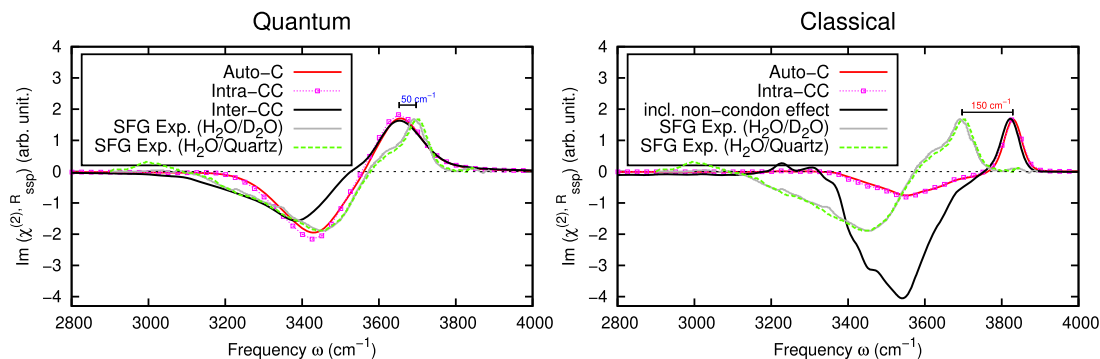


Figure 6. Simulated O-H stretch SFG spectra of the water/air interface, with NQE (quantum simulation) and without (classical simulation). For the sake of comparison, the classical simulation was performed with the same computational details as the quantum simulation. However, in the classical simulation the intermolecular cross-correlation term is neglected due to the shorter simulation time (~ 40 ps), but as is common practice in classical MD simulations, non-Condon effects were included to enhance the H-bonded O-H peak.

enhancement that is in better agreement with experiment. The latter is due to the fact that the SFG spectra of Figure 5 includes the small but apparently significant contributions of L_2 . As can be seen in Figure 4, a new positive peak appears at 3200 cm^{-1} , whereas the dangling O-H peak is vanishing, indicating that single H-donor water molecules are absent in L_2 . More importantly, the positive peak of L_2 entails to cancellation with the corresponding peak of L_1 leading to a reduction of the overall SFG signal at 3200 cm^{-1} in agreement with experimental measurements [21].

The impact of NQE can be clearly seen in Figure 6, showing that the inclusion of NQE leads to a blue-shift of $\sim 50\text{ cm}^{-1}$ with respect to experimental SFG measurements, whereas neglecting NQE entails a red-shift of $\sim 150\text{ cm}^{-1}$. This is to say that NQE makes up for a blue-shift of as much as $\sim 200\text{ cm}^{-1}$ that is a well known phenomenon and have already been reported by previous studies [30,56–58]. Yet, neglecting NQE, non-Condon or many-body effects are necessary to obtain good agreement with experimental SFG measurements in terms of the intensities within the H-bonded O-H peak region [11,30].

To study the origin behind the intermolecular vibrational contribution in our SFG spectra, we have separated the intermolecular contribution, which originates from the interfacial water molecules, from the vibrational coupling between the bulk and interfacial water molecules. For that purpose, we distinguish between intralayer and interlayer intermolecular coupling effects. As can be seen in Figure 7, the inclusion of the intermolecular cross-correlation term within the interfacial water layer (dotted green line), results in a slightly enhanced amplitude of the SFG signal at $3200\text{--}3380\text{ cm}^{-1}$ and a slightly reduced amplitude of the $3380\text{--}3600\text{ cm}^{-1}$ SFG peak. At the same time, these coupling effects entails a slight red-shift of the H-bonded O-H stretch frequency. However, only a

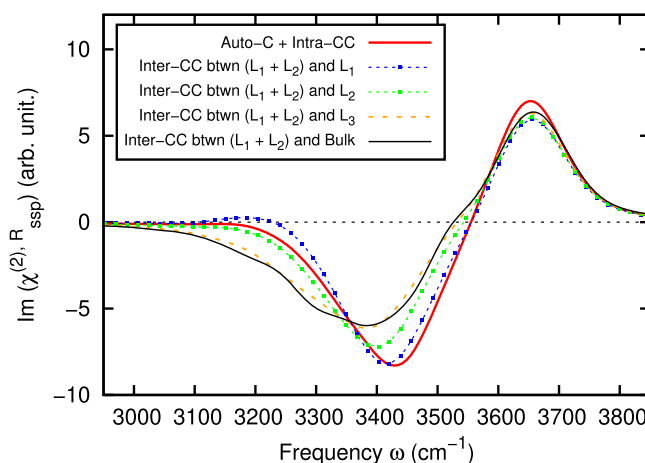


Figure 7. Simulated O-H stretch SFG spectra, where the intermolecular coupling effects are separated into intralayer and interlayer contributions. In addition, the SFG spectra including just Auto-C and Intra-CC, but no Inter-CC correlation terms is shown for comparison (red curve).

tiny enhancement of the $3350\text{--}3410\text{ cm}^{-1}$ SFG signal and a red-shift of $\sim 20\text{ cm}^{-1}$ can be attributed to the 2D H-bonded structure (located in L_1 , i.e. the dotted blue line), where the H-bonded network is oriented parallel to the instantaneous water surface [47,68,69]. This is to be expected, since the OH groups involved in such a H-bonded network can generate only a negligible SFG signature due to their orientation nearly parallel to the instantaneous water surface, which we believe is the reason for such a tiny enhancement and red-shift in the spectra. Yet, most intermolecular contributions are due to the interlayer coupling between the interfacial water and L_3 (dashed orange line), whereas the remaining contributions are originating mainly from the coupling between interfacial water layer and L_2 . In fact, this remaining contribution can be mainly attributed to the coupling

between water molecules in L_1 and L_2 , since the total intermolecular contribution from the water molecules of L_2 are very small, as is apparent in Figure 4. The interlayer coupling between more distant layers give rise to a tiny intermolecular contribution to the SFG spectra. All of these results clearly suggest that the intermolecular vibrational contributions in the SFG spectra of water/air interface are governed by the coupling between the SFG active interfacial layer and the SFG inactive centrosymmetric bulk layer.

To elucidate the relationship between the intermolecular vibrational contributions in the SFG spectra and the H-bonding network at the water/air interface, we plot the Inter-CC function corresponding to non-donor (ND), single-donor (SD) and double-donor (DD) water configurations separately, as shown in Figure 8. We find that most of the intermolecular contributions are coming from the intermolecular coupling between DD and DD water configurations (black line), whereas the remaining contributions come from the intermolecular coupling between SD and DD water motifs (orange line). The intermolecular coupling between SD and SD water configurations (yellow line) are insignificant for the SFG spectra. Moreover, since the population of ND water motifs are very small at the interface [46], they also are not able to contribute to the spectra. These results clearly suggests that the intermolecular contributions to the SFG spectra are governed by intermolecular coupling effects between DD and DD water, as well as between SD and DD water configurations, which is consistent with previous works of others [31,38,39,68,70].

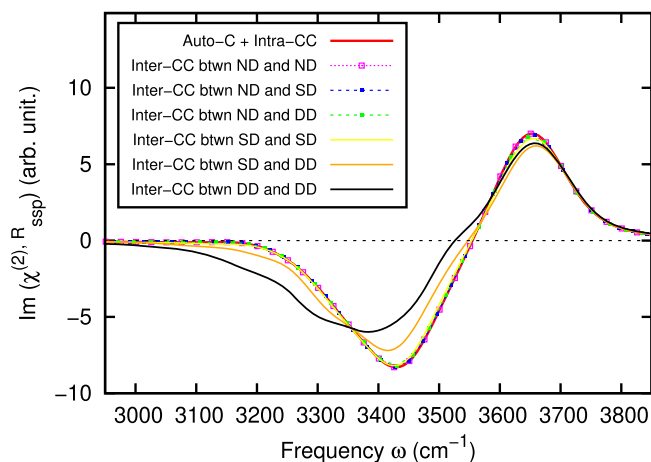


Figure 8. Simulated O-H stretch SFG spectra, where the different Inter-CC contributions are shown as a function of the H-bond network of the interfacial water molecules. In addition, the SFG spectra including just Auto-C and Intra-CC, but no Inter-CC correlation terms is shown for comparison (red curve).

4. Conclusion

We have investigated the impact of intermolecular vibrational coupling effects on the O-H stretch modes in SFG spectra of the water/air interface. We find that these intermolecular coupling effects, as determined using the intermolecular cross-correlation term, induces a red-shift of the H-bonded O-H stretch peak by $\sim 50 \text{ cm}^{-1}$. Moreover, they also entail a somewhat decreased SFG signal between $3380\text{--}3600 \text{ cm}^{-1}$, while, at the same time, leading to an enhanced amplitude at $3000\text{--}3380 \text{ cm}^{-1}$. Including these intermolecular coupling effects, leads to systematically improved SFG spectra that are in much better agreement with experimental measurements. Our investigation also shows that the inclusion of intermolecular coupling effects within the first three water layers, i.e. from the water/air interface up to a distance of 6 \AA , is essential to quantitatively reproduce experimental SFG spectra. Even though this comes at the price of a somewhat slower convergence with respect to trajectory length (100 ps for $r_t \leq 2 \text{ \AA}$, but 500 ps for $r_t \geq 6 \text{ \AA}$), we nevertheless believe that the inclusion of these effects should be taken into account in future SFG simulations. Furthermore, based on an instantaneous layer analysis to isolate the contribution of the individual water layer, we find that the intermolecular vibrational contribution to the SFG spectra of the water/air interface is dominated by the coupling between the SFG active interfacial water molecules and SFG inactive bulk water, whereas more distant coupling effects are inessential. Most of the intermolecular contributions within the SFG spectra are due to intermolecular coupling effects between DD and DD water structures, whereas the remaining contributions are mainly from the intermolecular vibrational coupling between SD and DD water motifs.

Acknowledgements

The authors would like to thank the Gauss Center for Supercomputing (GCS) for providing computing time through the John von Neumann Institute for Computing (NIC) on the GCS share of the supercomputer JUQUEEN at the Jülich Supercomputing Centre (JSC). The generous allocation of computing time on the FPGA-based supercomputer ‘Noctua’ by the Paderborn Center for Parallel Computing (PC²) is kindly acknowledged.

Disclosure statement

No potential conflict of interest was reported by the authors.

Funding

This project has received funding from the European Research Council (ERC) under the European Union’s Horizon 2020 research and innovation programme (grant agreement No

716142) and by the Federal Ministry of Education and Research of Germany (BMBF) in the framework of the german-swedish Röntgen-Ångström-Cluster 'SynXAS' (FKZ: 05K18PPA).

References

- [1] S. Narayan, J. Muldoon, M.G. Finn, V.V. Fokin, H.C. Kolb and K.B. Sharpless, *Angew. Chem. Int. Ed.* **44**, 3275 (2005).
- [2] C.M. Dobson, *Nature* **426**, 884 (2003).
- [3] B.J.F. Pitts, *Proc. Natl. Acad. Sci. USA* **107**, 6566 (2010).
- [4] J.Y. Luo, W.J. Cui, P. He and Y.Y. Xia, *Nat. Chem.* **2**, 760 (2010).
- [5] J.A. Killian and G.V. Heijne, *Trends Biochem. Sci.* **25**, 429 (2000).
- [6] G.L. Richmond, *Chem. Rev.* **102**, 2693 (2002).
- [7] L.R. Pratt and A. Pohorille, *Chem. Rev.* **102**, 2671 (2002).
- [8] Y.R. Shen and V. Ostroverkhov, *Chem. Rev.* **106**, 1140 (2006).
- [9] Y.R. Shen, *J. Phys. Chem. C* **116**, 15505 (2012).
- [10] A.G. Lambert, P.B. Davies and D.J. Neivandadt, *Appl. Spectrosc. Rev.* **40**, 103 (2005).
- [11] T. Ohto, K. Usui, T. Hasegawa, M. Bonn, and Y. Nagata, *J. Chem. Phys.* **143**, 124702 (2015).
- [12] A. Morita, *Chem. Phys. Lett.* **398**, 361 (2004).
- [13] Q. Du, E. Freysz and Y.R. Shen, *Phys. Rev. Lett.* **72**, 238 (1994).
- [14] Y. Nagata and S. Mukamel, *J. Am. Chem. Soc.* **132**, 6434 (2010).
- [15] M. Okuno and T. Ishibashi, *J. Phys. Chem. C* **119**, 9947 (2015).
- [16] S. Strazdaite, J. Versluis, E.H.G. Backus, and H.J. Bakker, *J. Chem. Phys.* **140**, 054711 (2014).
- [17] M. Hankett, Y. Liu, X. Zhang, C. Zhang and Z. Chen, *J. Polym. Sci., Part B: Polym. Phys.* **51**, 311 (2013).
- [18] J. Schaefer, E.H.G. Backus, Y. Nagata and M. Bonn, *J. Phys. Chem. Lett.* **7**, 4591 (2016).
- [19] Q. Du, R. Superfine, E. Freysz and Y.R. Shen, *Phys. Rev. Lett.* **70**, 2313 (1993).
- [20] N. Ji, V. Ostroverkhov, and Y.R. Shen, *Phys. Rev. Lett.* **100**, 096102 (2008).
- [21] S. Nihonyanagi, R. Kusaka, K. Inoue, A. Adhikari, S. Yamaguchi, and T. Tahara, *J. Chem. Phys.* **143**, 124707 (2015).
- [22] C. Hsieh, M. Okuno, J. Hunger, E.H.G. Backus, Y. Nagata and M. Bonn, *Angew. Chem., Int. Ed.* **53**, 8146 (2014).
- [23] S. Yamaguchi, *J. Chem. Phys.* **143**, 034202 (2015).
- [24] M.G. Brown, E.A. Raymond, H.C. Allen, L.F. Scatena and G.L. Richmond, *J. Phys. Chem. A* **104**, 10220 (2000).
- [25] S. Nihonyanagi, T. Ishiyama, T.K. Lee, S. Yamaguchi, M. Bonn, A. Morita and T. Tahara, *J. Am. Chem. Soc.* **133**, 16875 (2011).
- [26] F. Perakis, L.D. Marco, A. Shalit, F. Tang, Z.R. Kann, T.D. Kühne, R. Torre, M. Bonn and Y. Nagata, *Chem. Rev.* **116**, 7590 (2016).
- [27] R. Khatib and M. Sulpizi, *J. Phys. Chem. Lett.* **8**, 1310 (2017).
- [28] M. Sulpizi, M. Salanne, M. Sprik and M.P. Gaigeot, *J. Phys. Chem. Lett.* **4**, 83 (2013).
- [29] T. Ishiyama, H. Takahashi, and A. Morita, *J. Phys.: Condens. Matter* **24**, 124107 (2012).
- [30] G.R. Medders and F. Paesani, *J. Am. Chem. Soc.* **138**, 3912 (2016).
- [31] D.R. Moberg, S.C. Straight and F. Paesani, *J. Phys. Chem. B* **122**, 4356 (2018).
- [32] A. Morita and J.T. Hynes, *Chem. Phys.* **258**, 371 (2000).
- [33] T. Ishiyama and A. Morita, *Annu. Rev. Phys. Chem.* **68**, 355 (2017).
- [34] T. Ishiyama and A. Morita, *J. Phys. Chem. C* **113**, 16299 (2009).
- [35] A. Morita and J.T. Hynes, *J. Phys. Chem. B* **106**, 673 (2002).
- [36] B.M. Auer and J.L. Skinner, *J. Chem. Phys.* **129**, 214705 (2008).
- [37] M. Sovago, R.K. Campen, G.W.H. Wurpel, M. Muller, H.J. Bakker, and M. Bonn, *Phys. Rev. Lett.* **100**, 173901 (2008).
- [38] Y. Ni and J.L. Skinner, *J. Chem. Phys.* **145**, 031103 (2016).
- [39] C.J. Tainter, Y. Ni, L. Shi and J.L. Skinner, *J. Phys. Chem. Lett.* **4**, 12 (2013).
- [40] J.H. Choi and M. Cho, *J. Chem. Phys.* **138**, 174108 (2013).
- [41] C. Zhang, R.Z. Khaliullin, D. Bovi, L. Guidoni and T.D. Kühne, *J. Phys. Chem. Lett.* **4**, 3245 (2013).
- [42] T.D. Kühne and R.Z. Khaliullin, *Nat. Commun.* **4**, 1450 (2013).
- [43] B.M. Auer and J.L. Skinner, *J. Chem. Phys.* **128**, 224511 (2008).
- [44] T. Ohto, H. Tada and Y. Nagata, *Phys. Chem. Chem. Phys.* **20**, 12979 (2018).
- [45] T. Ohto, E.H.G. Backus, C.S. Hsieh, M. Sulpizi, M. Bonn and Y. Nagata, *J. Phys. Chem. Lett.* **6**, 4499 (2015).
- [46] T.D. Kühne, T.A. Pascal, E. Kaxiras and Y. Jung, *J. Phys. Chem. Lett.* **2**, 105 (2011).
- [47] J. Kessler, H. Elgabarty, T. Spura, K. Karhan, P. Partovi-Azar, A.A. Hassanali and T.D. Kühne, *J. Phys. Chem. B* **119**, 10079 (2015).
- [48] T.D. Kühne, *WIREs Comput. Mol. Sci.* **4**, 391 (2014).
- [49] T.D. Kühne, M. Krack, F.R. Mohamed, and M. Parrinello, *Phys. Rev. Lett.* **98**, 066401 (2007).
- [50] D. Chandler and P.G.J. Wolynes, *J. Chem. Phys.* **74**, 4078 (1981).
- [51] M. Parrinello and A. Rahman, *J. Chem. Phys.* **80**, 860 (1984).
- [52] S. Habershon, T.E. Markland, and D.E. Manolopoulos, *J. Chem. Phys.* **131**, 024501 (2009).
- [53] M. Parrinello and A. Rahman, *Phys. Rev. Lett.* **45**, 1196 (1980).
- [54] C.J. Tainter, P.A. Pieniazek, Y. Lin, and J.L. Skinner, *J. Chem. Phys.* **134**, 184501 (2011).
- [55] J.L.F. Abascal and C. Vega, *J. Chem. Phys.* **123**, 234505 (2005).
- [56] D. Ojha, A. Henao, and T.D. Kühne, *J. Chem. Phys.* **148**, 102328 (2018).
- [57] M. Rossi, M. Ceriotti, and D.E. Manolopoulos, *J. Chem. Phys.* **140**, 234116 (2014).
- [58] T. Spura, C. John, S. Habershon and T.D. Kühne, *Mol. Phys.* **113**, 808 (2015).
- [59] A. Köster, T. Spura, G. Rutkai, J. Kessler, H. Wiebeler, J. Vrabcac and T.D. Kühne, *J. Comput. Chem.* **37**, 1828 (2016).
- [60] C. John, T. Spura, S. Habershon, and T.D. Kühne, *Phys. Rev. E* **93**, 043305 (2016).
- [61] L.B. Partay, G. Hantal, P. Jedlovsky, A. Vincze and G. Horvai, *J. Comput. Chem.* **29**, 945 (2008).

- [62] P. Tarazona and E. Chacon, *Phys. Rev. B* **70**, 235407 (2004).
- [63] G. Hantal, P. Terlezky, G. Horvai, L. Nyulaszi and P. Jedlovszky, *J. Phys. Chem. C* **113**, 19263 (2009).
- [64] M. Sega, S.S. Kantorovich, P. Jedlovszky, and M. Jorge, *J. Chem. Phys.* **138**, 044110 (2013).
- [65] M. Matsumoto, Y. Takaoka and Y. Kataoka, *J. Chem. Phys.* **98**, 1473 (1993).
- [66] G.G. Lang, *ChemTexts* **1**, 1 (2015).
- [67] A.P. Willard and D. Chandler, *J. Phys. Chem. B* **114**, 1954 (2010).
- [68] S. Pezzotti, D.R. Galimberti and M.P. Gaigeot, *J. Phys. Chem. Lett.* **8**, 3133 (2017).
- [69] S. Pezzotti, A. Serva, and M.P. Gaigeot, *J. Chem. Phys.* **148**, 174701 (2018).
- [70] I.V. Stiopkin, C. Weeraman, P.A. Pieniazek, F.Y. Shalhout, J.L. Skinner and A.V. Benderskii, *Nature* **474**, 192 (2011).